Heat transfer analysis of reactive boundary layer flow over a wedge in a nanofluid using Buongiorno's model

Cite as: AIP Advances 14, 115002 (2024); doi: 10.1063/5.0237487
Submitted: 5 September 2024 • Accepted: 18 October 2024 •
Published Online: 4 November 2024

Saeed Ullah Jan,[1] Aatif Ali,[2,a)] Mohamed Sharaf,[3] and Joshua Kiddy K. Asamoah[4,5,a)]

AFFILIATIONS

[1] Department of Mathematics, COMSATS University Islamabad, Abbottabad, Pakistan
[2] School of Mathematical Sciences, Jiangsu University, Zhenjiang, Jiangsu 212013, P.R. China
[3] Industrial Engineering Department, College of Engineering, King Saud University, P.O. Box 800, Riyadh 11421, Saudi Arabia
[4] Department of Mathematics, Saveetha School of Engineering SIMATS, Chennai, India
[5] Department of Mathematics, Kwame Nkrumah University of Science and Technology, Kumasi, Ghana

[a)] **Authors to whom correspondence should be addressed:** atifkh98@gmail.com and jkkasamoah@knust.edu.gh

ABSTRACT

The reactive two-dimensional steady laminar boundary layer flow over a wedge is examined in this work, with an emphasis on the mass and heat transfer of nanofluids. This study investigates the effects of three different chemical reactions—Arrhenius, bimolecular, and sensitized reactions—using Buongiorno's model. Through similarity transformations, the system of partial differential equations (PDEs) is converted into ordinary differential equations, which are then solved by combining the shooting method with the Runge–Kutta–Fehlberg numerical technique. The findings show that the skin friction coefficient is greatly increased by raising the pressure gradient and stretching/contracting wedge parameters. On the other hand, as the thermophoresis parameter, Brownian motion parameter, activation energy, and Lewis number increase, the Nusselt number decreases, signifying a decrease in the efficiency of heat transfer. A higher Sherwood number, on the other hand, indicates increased mass transfer and is brought about by increases in the Lewis number, thermophoresis parameter, activation energy, and Falkner–Skan power-law parameter. These findings provide important information for maximizing heat and mass transfer in nanofluid systems. Key values for the skin friction coefficient, local Nusselt number, and the Sherwood number are given in tabular form, and the results are graphically represented.

NOMENCLATURE

C_0	Initial concentration of reactant species
D_B	Brownian motion coefficient
D_T	Thermophoresis coefficient
h	Planck's number
J	Rate constant
k	Boltzmann's constant
k	The material parameter
n	Exponent
Q	Heat of reaction
R	Universal gas constant
α	Thermal diffusivity (m^2 s^-1)
η	Dimensionless similarity variable
μ	Dynamic viscosity of the fluid (kg m^{-1} s^{-1})
ρ	Density of nanofluid (kg m^{-3}) $[ML^{-3}]$
$(\rho)_f$	Density of the base fluid (kg $m^{-3)}$ $[ML^{-3}]$
$(\rho c)_f$	Heat capacity of the base fluid (J kg K) [L TΘ]
$(\rho cp)_p$	Specific heat of the nanoparticle (J kg K) [L TΘ]
$\tilde{u}$, $\tilde{v}$	Velocity (m/sec) components in x and y-directions
σ	Electric conductivity $\left(\text{ohm}^{-1}\text{m}^{-1}\right)$ $[M^{-2}L^{-3}T^3A^2]$
τ	Parameter defined by $\frac{(\rho c)_p}{(\rho c)_f}$
υ	Kinematic viscosity (m^2 s^{-1}) $[L^2T^{-1}]$
υ_1	Vibration frequency

I. INTRODUCTION

Falkner and Skan[1] studied a steady laminar stream past a fixed wedge in order to illustrate Prandtl's boundary layer theory. They reduced the boundary layer equations to an ordinary differential equation—the Falkner–Skan equation—by implementing a similarity transformation. The boundary layer equations are parabolic in nature and are usually regarded as a suitable representation of the flows described by the Falkner–Skan solutions. As mentioned by Banks *et al.*,[2] the solutions are believed to be valid in an asymptotic sense, but this method typically does not account for initial conditions. Riley and Weidman[3] and Ishak *et al.*[4] in their papers investigated the Falkner–Skan equation for different geometries and fluid models, where the boundary velocity and the external velocity both follow the identical power rule with respect to the downstream distance. The thermal processing of materials that resemble sheets is one of the many engineering applications where an understanding of boundary layer behavior over a stirring incessant compact apparatus is essential. Plastic film drawing, fine-fiber mats, etc., are among the products that depend on this process. Improving heat transfer is essential to increasing electronic device performance and compactness. Because of their comparatively low thermal conductivity, traditional cooling agents are not as effective at transferring heat. These fluids are combined with tiny particles to produce what are referred to as nanofluids, which have improved thermal properties. The concentration and form of the particles determine the physical and chemical characteristics of these nanoparticle suspensions. It has been discovered that a base fluid's thermal conductivity can be greatly increased by adding a small amount of nanoparticles to it. The thermal dispersion effect, which is produced by the random measure of nanoparticles and interactions among the elements and the fluid, speeds up the fluid's rate of energy exchange. The efficiency of heat transfer can be increased overall by using nanoparticles to regulate different fluid parameter attributes. A pioneer in the field of nanoparticle research, Choi[5] talked about how these particles impact a fluid's thermal conductivity. Buongiorno[6] expanded on the model for nanofluids, emphasizing the functions of thermophoresis and Brownian motion in defining their physical characteristics. Xuan and Roetzel[7] studied the analysis of heat transfer in different models for nanofluids. Assiri[8] discussed the convectional force of a porous wedge. The numerical investigation of hyperbolic and hybrid nanofluids is performed in Refs. 9 and 10. The effects of incorporating nanoparticles into lubricating oils and refrigerants were investigated by Saidur *et al.*[11] They examined the effects of these suspensions of nanoparticles on the effectiveness and functionality of the systems. The nanoparticles have the potential to improve system performance by augmenting the thermal conductivity and heat transfer properties. The study emphasized how employing nanofluids in refrigeration could improve energy efficiency. The development of more sustainable and effective refrigeration technologies depends on this research. According to Mahian *et al.*[12] and Behar *et al.*,[13] recent thorough reviews of the most recent developments in nanofluid research for heat transfer applications have been completed. Reactive flows are chemically driven and have a wide range of uses, such as in combustion processes and natural phenomena found in Earth's atmosphere and oceans. Heat explosion theory's basic ideas were first presented by Semenov and Frank-Kamenetskii. Frank-Kamenetskii[14] developed a stability criterion for perfect wall reactors and investigated heat transfer in chemical kinetics. Reactive flows in parallel plates and horizontal cylinders were studied by Haroon and Siddiqui *et al.*,[15,16] who looked at three chemical reactions in the framework of a power-law fluid model. Some studies[17–26] provide more details on reactive flows, while some studies[27–33] show how interested researchers are in the study of reactive nanofluid particles and fluid flow with some effects through intelligent computing. The review of the literature reveals that no studies have been done on reactive nanofluid boundary layer streams past a wedge. It is noteworthy that the unique physical and chemical properties of materials at the nanoscale have led to the widespread application of nanotechnology in conjunction with chemical reactions in industry. This study uses similarity transformation to convert the system of partial differential equations into a system of ordinary differential equations (ODEs) using Buongiorno's nanofluid model. The RK–Fehlberg method is then applied to solve the resulting ODEs. Using graphs and tables, the effects of different physical parameters are investigated and displayed.

II. PROBLEM STATEMENT

The problem is to study the boundary layer flow over an impermeable wedge in a reactive nanofluid that stretches at a velocity of $u_w(x)$. Here, $u_w(x) > 0$ stands for a wedge surface that is stretching, and $u_w(x) < 0$ stands for a wedge surface that is contracting. In addition, $U_e(x)$ is the free stream velocity along the x-axis of the wedge as displayed in Fig. 1. Using Buongiorno's model, this study examines three chemical reactions that occur within the reactive nanofluid. It is assumed that the concentration of nanoparticles $\tilde{C}$ and the temperature $\tilde{T}$ have constant values of C_w and T_w, respectively, at the stretching surface. As y gets closer to infinity, the surrounding temperature and concentration are represented by the letters T_∞ and C_∞, respectively. Using all these presumptions allow us to formulate the basic governing equations for reactive nanofluids as follows:[12,25]

$$\frac{\partial \tilde{u}}{\partial x} + \frac{\partial \tilde{v}}{\partial y} = 0, \tag{1}$$

$$\tilde{u}\frac{\partial \tilde{u}}{\partial x} + \tilde{v}\frac{\partial \tilde{u}}{\partial y} = U_e\frac{dU_e}{dx} + \nu\frac{\partial^2 \tilde{u}}{\partial y^2}, \tag{2}$$

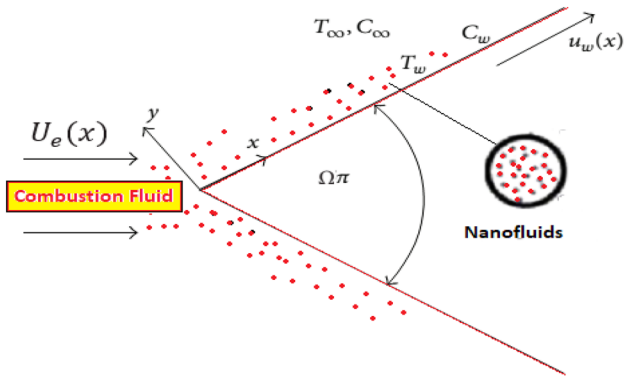

FIG. 1. Geometry of the problem.

$$\tilde{u}\frac{\partial \tilde{T}}{\partial x}+\tilde{v}\frac{\partial \tilde{T}}{\partial y}=\alpha\frac{\partial^2 \tilde{T}}{\partial y^2}+\tau\left[D_B\frac{\partial \tilde{T}}{\partial y}\frac{\partial \tilde{C}}{\partial y}+\frac{D_T}{T_\infty}\left(\frac{\partial \tilde{T}}{\partial y}\right)^2\right], \tag{3}$$

$$\tilde{u}\frac{\partial \tilde{C}}{\partial x}+\tilde{v}\frac{\partial \tilde{C}}{\partial y}=D_B\frac{\partial^2 \tilde{C}}{\partial y^2}+\frac{D_T}{T_\infty}\frac{\partial^2 \tilde{T}}{\partial y^2}+QC_0K_0\left(\tilde{T}\right), \tag{4}$$

with the boundary conditions being

$$\begin{aligned}\tilde{u}=u_w(x)=-\lambda U_e(x),\ \tilde{v}=0,\ \tilde{T}=T_w,\ \tilde{C}=C_w \quad \text{at} \quad y=0,\\ \tilde{u}=U_e(x),\ \tilde{T}=T_\infty,\ \tilde{C}=C_\infty \quad \text{as} \quad y\to\infty,\end{aligned} \tag{5}$$

where $QC_0K_0\left(\tilde{T}\right)$ is the chemical reaction term and defined in Refs. 13 and 14.

Here, $K_0\left(\tilde{T}\right)=J\left(\frac{kT}{v_1h}\right)^n e^{\left(\frac{-E}{RT}\right)}$.

We introduce the dimensionless similarity transformations as follows:

$$u_w(x)=ax^m, U_e(x)=cx^m,$$

$$\left.\begin{aligned}\eta=\sqrt{\frac{(1+m)U_e}{2xv}}y, \quad \psi=\sqrt{\frac{2U_exv}{1+m}}F(\eta),\\ \theta=\frac{T-T_\infty}{T_w-T_\infty}, \quad \phi=\frac{C-C_\infty}{C_w-C_\infty}.\end{aligned}\right\} \tag{6}$$

Here, ψ is the stream function, $\tilde{u}=\frac{\partial\psi}{\partial y}$ and $\tilde{v}=-\frac{\partial\psi}{\partial x}$. Using Eq. (6) in Eqs. (1)–(5), we have a system of equations along with boundary conditions,

$$F'''+FF''+\Omega\left(1-F'^2\right)=0, \tag{7}$$

$$\theta''+\Pr\left(F\theta'+Nb\phi'\theta'+Nt\theta'^2\right)=0, \tag{8}$$

$$\phi''+LeF\phi'+\frac{Nt}{Nb}\theta''-\delta f(\theta;\beta,n)=0, \tag{9}$$

$$\left.\begin{aligned}F(\eta)=0,\ F'(\eta)=-\lambda,\ \theta(\eta)=1,\ \phi(\eta)=1 \quad \text{at} \quad \eta=0,\\ F'(\eta)=1,\ \theta(\eta)=0,\ \phi(\eta)=0 \quad \text{as} \quad \eta\to\infty,\end{aligned}\right\} \tag{10}$$

where the parameters are defined as

$$\left.\begin{aligned}\Omega=\frac{2m}{1+m},\ \Pr=\frac{v}{\alpha},\ Le=\frac{v}{D_B},\ \delta=\frac{QEC_\infty k^nT_\infty^{n-2}}{v^nh^nRK}e^{\frac{-E}{RT}},\\ f(\theta;\beta,\ n)=(1+\beta\theta)^ne^{\left(\frac{\theta}{1+\beta\theta}\right)},\ Nt=\frac{\tau D_T(T_w-T_\infty)}{T_\infty v},\\ Nb=\frac{\tau D_B(C_w-C_\infty)}{T_\infty v}.\end{aligned}\right\} \tag{11}$$

The Falkner–Skan power-law parameter is denoted as m, and the Hartree pressure gradient is represented by Ω. A boundary layer separation is indicated when $m<0$, while a favorable pressure gradient is indicated when $m>0$. The moving wedge parameter is defined by $\lambda=\frac{a}{c}$, given two constants a and c. Within the framework of a wedge, a stretching wedge is denoted by $\lambda<0$, a contracting wedge is denoted by $\lambda>0$, and a fixed wedge is denoted by $\lambda=0$.

The physical quantities of engineering interest are the skin friction coefficient C_f, local Nusselt number Nu_x, and local Sherwood number Sh_x and are defined as

$$\begin{aligned}C_f=\frac{2\mu_f}{\rho U^2{}_e(x)}\left(\frac{\partial u}{\partial y}\right)_{y=0}, Nu_x=\frac{-xk_f}{k(T_w-T_\infty)}\left(\frac{\partial T}{\partial y}\right)_{y=0},\\ Sh_x=\frac{-x}{(C_w-C_\infty)}\left(\frac{\partial C}{\partial y}\right)_{y=0}.\end{aligned} \tag{12}$$

The non-dimensional form of Eq. (12) is given by

$$\begin{aligned}(Re_x)^{1/2}C_f=2\left(\frac{m+1}{2}\right)^{1/2}F''(0),\\ (Re_x)^{-1/2}Nu_x=-\left(\frac{m+1}{2}\right)^{\frac{1}{2}}\theta'(0),\\ (Re_x)^{-1/2}Sh_x=-\left(\frac{m+1}{2}\right)^{\frac{1}{2}}\phi'(0).\end{aligned} \tag{13}$$

III. NUMERICAL SOLUTION

Equations (7)–(9) and the corresponding boundary conditions in Eq. (10) were solved numerically by combining the shooting technique with the Runge–Kutta–Fehlberg method. In order to guarantee that the solution converged across all pertinent variables in the system of equations, a suitable parameter η_∞ was selected. In order to achieve accuracy to the fifth decimal place, this parameter was chosen to aid with convergence. This method guaranteed the numerical solution's accuracy and stability. We used a combination of the shooting technique and the RK–Fehlberg method, where convergence is dependent on a number of factors, such as the particular problem being addressed, the numerical parameters that are selected, and the initial conditions. The RK–Fehlberg method is highly regarded for its strong convergence properties, which make it particularly useful when dealing with ODEs. It uses adaptive step sizes to ensure convergence and maintain accuracy even when dealing with stiff ODEs. Nonetheless, the reactive nanofluid problem's ODE behavior and chosen tolerances may still have an impact on convergence. The accuracy of the initial estimates of the boundary conditions and the behavior of the ODEs at the boundaries determine how well the shooting technique converges and flow chat of the scheme is shown in (Fig. 2).

IV. RESULTS AND DISCUSSIONS

The graphs in this section illustrate how different factors affect the temperature $\theta(\eta)$, concentration $\phi(\eta)$, and velocity $F'(\eta)$ profiles. The Prandtl number, Pr = 6.2, is maintained constant in these computations. The range for different parameters is as follows: pressure gradient parameter $1\le\Omega\le4$, shrinking/stretching wedge parameter $-1\le\lambda\le1$, $0\le m\le1$, thermophoresis parameter $0.0\le Nt\le0.9$, Brownian motion parameter $0.0\le Nb\le0.9$, Lewis number $0.0\le Le\le2.0$, activation energy parameter $1.0\le\beta\le4$, and Frank-Kamenetskii number $0\le\delta\le2$, and for three different chemical reactions, we have $n=0, n=0.5, n=-2$. Figures 3–13 show the significance of variations in various parameters on the profiles of temperature, concentration, and velocity. As the pressure gradient parameter increases, so does the wedge's velocity, as seen in Fig. 3.

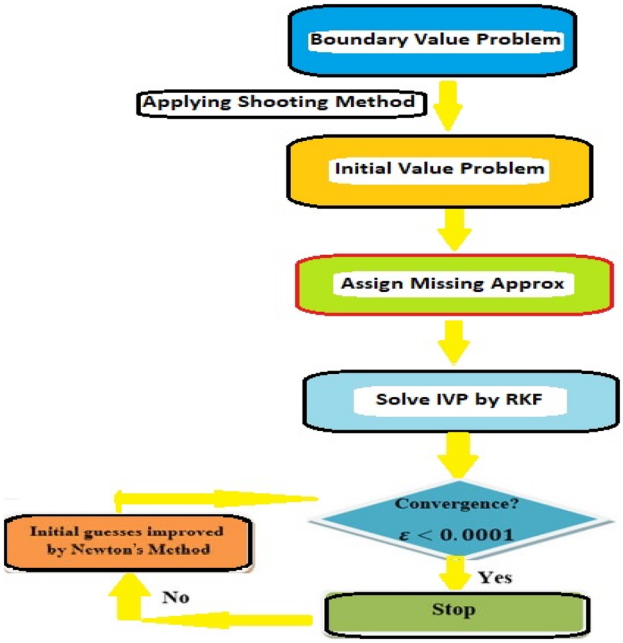

FIG. 2. Flow chart of numerical methods.

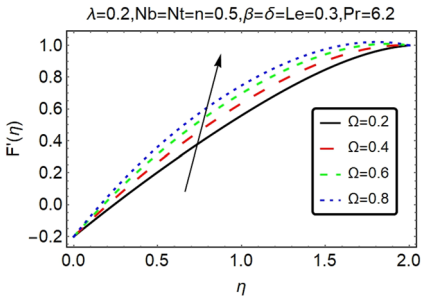

FIG. 3. Velocity outlines for different values of Ω, with $0 \le m \le 1$.

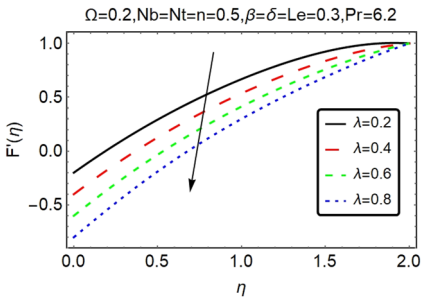

FIG. 4. Velocity outlines for numerous λ, contracting wedge $\lambda > 0$.

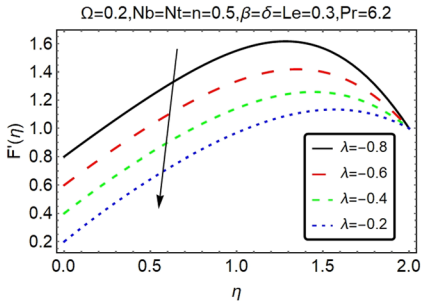

FIG. 5. Velocity outlines for numerous λ, stretching wedge $\lambda < 0$.

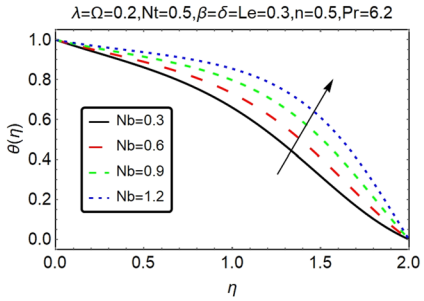

FIG. 6. Temperature curves for different values of *Nb*.

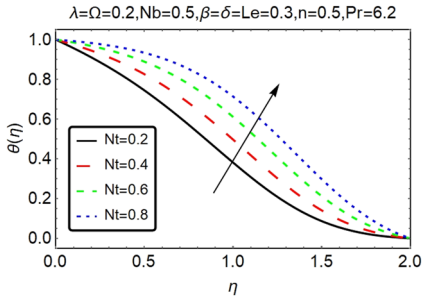

FIG. 7. Temperature curves for different values of *Nt*.

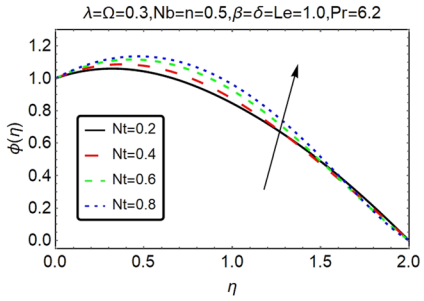

FIG. 8. Concentration profiles for various *Nt*.

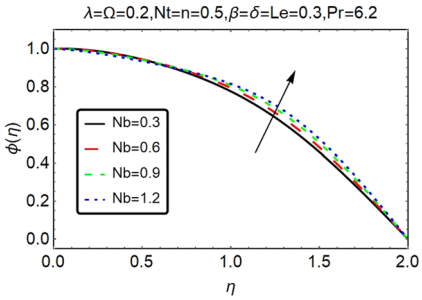

FIG. 9. Concentration profiles for various *Nb*.

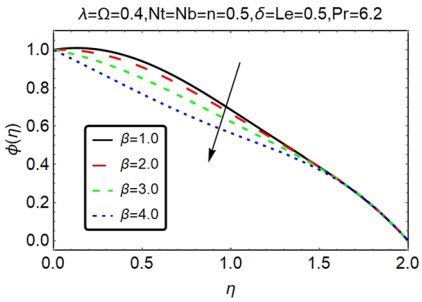

FIG. 10. Concentration profiles for various β.

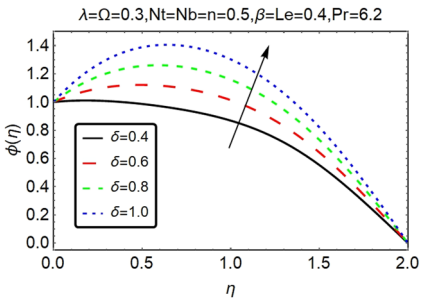

FIG. 11. Concentration profiles for numerous δ.

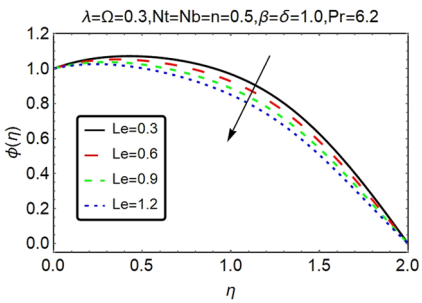

FIG. 12. Concentration profiles for numerous *Le*.

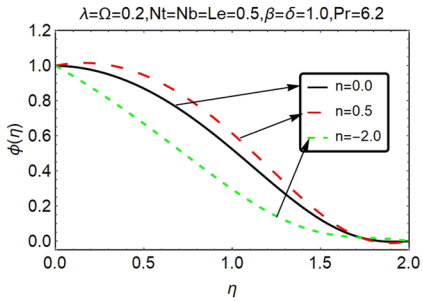

FIG. 13. Concentration profiles for $n = 0, n = 0.5, n = -2$.

The reason for this is that the boundary layer tends to be thinner and less likely to be split, which increases the wedge's velocity. Figures 4 and 5 illustrate the impact of the shrinking/stretching wedge parameter λ. As the shrinking wedge parameter $\lambda > 0$ increases, velocity decreases. An unfavorable pressure gradient that is perpendicular to the direction of flow may arise as the wedge contracts. This happens as a result of the fluid having to overcome the contracting surface's added resistance. Stretching, $\lambda < 0$, can create unfavorable pressure gradients in the boundary layer, where the pressure rises along the flow direction, further slowing down the flow as the fluid must overcome this resistance. This can cause a decrease in velocity within the boundary layer in a flow over a stretching wedge. These effects produce a thicker boundary layer and may lead to separation or flow instabilities, which will have a major effect on the velocity profile. The effect of variation of *Nb* on the temperature distribution is displayed in Fig. 6. Because of the enhanced thermal conductivity and energy transport made possible by the random motion of nanoparticles, the temperature profile within the boundary layer rises as the *Nb* rises. As a result, the boundary layer's temperature distribution rises and heat transfer becomes more effective.

Figure 7 shows how the thermophoresis parameter *Nt* affects the temperature distribution. The primary cause of the temperature profile rise with the rise in the thermophoresis parameter is the improved migration of particles from hotter to cooler regions, which leads to increased thermal energy transport and more effective heat redistribution. Higher temperature profiles and better heat transfer properties result from this. The outcome of *Nt* on the concentration profile is plotted in Fig. 8. The movement and accumulation of particles caused by temperature gradients is principally responsible for the increase in the concentration profile within the boundary layer that occurs with an increase in the thermophoresis parameter. A higher concentration profile results from this migration's enhancement of the mass transfer and concentration gradient processes. The impact of *Nb* on the concentration profile is displayed in Fig. 9. A rise in *Nb* denotes a greater intensity of particle movement and increased diffusion. It can also result in an increase in the concentration profile. More even particle distribution throughout the boundary layer is made possible by this improved diffusion.

The impact of the activation energy parameter on the concentration profiles is shown in Fig. 10, where the concentration profiles decrease as the activation energy parameter increases. It serves as an energy barrier that must be crossed by reactants in order

to change into products. Reaction rate falls with increasing activation energy parameter. This results in a higher concentration of unreacted species within the boundary layer because fewer reactant molecules are transformed into products. The effects of the Frank-Kamenetskii number δ on the concentration profile are displayed in Fig. 11. A dimensionless metric used in combustion and chemical reaction analysis is the Frank-Kamenetskii number. It shows the relationship between the heat produced by a chemical reaction and the heat lost through conduction. The concentration profile increases with an increase in the Frank-Kamenestskii parameter. The concentration gradient within the boundary layer is raised by the increased reaction rate, which facilitates a greater mass transfer and raises the concentration profile even more. The impact of the Lewis number *Le* on concentration profiles is depicted in Fig. 12. Because heat diffuses more quickly at higher temperatures, any temperature-dependent reactions or processes can be impacted, resulting in a faster thermal equilibrium than concentration equilibrium as the concentration profile rises. Three distinct chemical reactions and their effects on the concentration profiles are shown in Fig. 13. When $n = 0$, the reaction is described by an Arrhenius or zero-order kinetic model, in which the rate of reaction is unaffected by the reactant concentration. When $n = 0.5$, two reactant molecules are present in sufficient concentration and the rate of the reaction is bimolecular. Finally, if $n = -2$, the reaction is sensitized, meaning that a sensitizing agent has an impact on the rate and has changed the standard concentration dependency.

A comparison between our current results for the skin friction coefficient and the Nusselt number and those from earlier research for different values of m is shown in Tables I and II. The strong agreement between the obtained results and the extant literature suggests that our computations were accurate and consistent.

Table III shows that as the stretching/contracting wedge parameter and the pressure gradient parameter increase, so does the skin friction coefficient. This suggests that increased frictional forces at the boundary layer are caused by higher pressure gradients and greater stretching or contraction of the wedge surface. The Nusselt number Nu_x is examined for a number of parameters in Table IV.

TABLE I. Comparison of $f''(0)$ with the previous literature when $\beta = \lambda = \delta = 0$.

m	Yacob *et al.*[17]	White[18]	Khan and Pop[19]	Present results
0	0.469 72	0.469 72	0.469 72	0.469 72
0.090	0.655 00	0.655 10	0.655 10	0.655 10
0.20	0.802 23	0.802 23	0.802 24	0.802 24
0.33	0.927 64	0.927 71	0.927 71	0.927 71
0.5	⋯	1.038 94	1.038 94	1.038 94
1	1.232 63	1.232 64	1.232 64	1.232 64

TABLE II. Comparison of $-\theta'(0)$ with the previous literature when $\lambda = \delta = Nt = \beta = Nb = 0$.

m	Khan and Pop[19]	Kuo[20]	Blasius[21]	Present results
0	0.8769	0.8668	0.8670	0.8770
1	1.1279	1.1147	1.1152	1.1279

TABLE III. Variation of skin friction coefficient with numerous parameters.

m	λ	$(Re_x)^{1/2}C_f$
0.2	0.5	1.715 94
0.4		2.059 12
0.6		2.366 94
0.8		2.643 81
0.5	0.2	1.892 11
	0.4	2.004 70
	0.6	2.148 64
	0.8	2.317 59
0.5	−0.8	1.814 75
	−0.6	1.843 52
	−0.4	1.905 59
	−0.2	1.992 39

TABLE IV. Variation of Nusselt and Sherwood numbers with different parameters.

m	Nt	Nb	Le	β	n	$(Re_x)^{-1/2}Nu_x$	$(Re_x)^{-1/2}Sh$
0.2	0.5	0.5	0.5	1.0	0.5	0.049 180	−0.135 72
0.4						0.068 390	−0.124 58
0.6						0.088 673	−0.116 50
0.8						0.108 448	−0.110 66
0.3	0.3	0.5	0.5	1.0	0.5	0.058 533	−0.129 72
	0.5					0.024 725	0.081 176
	0.7					0.009 814 3	0.297 60
	0.9					0.003 705	0.512 50
0.5	0.4	0.1	0.5	0.5	0.5	0.073 794	0.001 338
		0.3				0.044 758	−0.200 87
		0.5				0.023 246	−0.279 52
		0.7				0.010 437	−0.322 34
0.3	0.3	0.3	0.5	1.0	0.5	0.058 533	−0.129 72
				2.0		0.056 313	−0.039 974
				3.0		0.052 196	0.116 68
				4.0		0.046 722	0.336 62
0.5	0.5	0.5	0.3	1.0	0.5	0.059 519	−0.131 35
			0.5			0.058 533	−0.129 72
			0.7			0.057 633	−0.128 78
			0.9			0.056 809	−0.128 45
0.5	0.5	0.5	0.5	1.0	0.0	0.049 968	0.127 38
					0.5	0.058 533	−0.129 72
					−2.0	0.039 241	0.456 68

The Nusselt number increases with an increase in the parameter m. On the other hand, a decrease in the Nusselt number indicates a decrease in heat transfer efficiency and is brought on by increases in the thermophoresis parameter Nt, Brownian motion parameter Nb, activation energy parameter β, and Lewis number Le. The table also looks at how various parameters affect the mass transfer metric known as the Sherwood number. Higher values of the Lewis number, thermophoresis parameter, activation energy parameter, and m all result in an increase in the Sherwood number, which denotes a better mass transfer. Nevertheless, as the Brownian motion parameter increases, it decreases.

V. CONCLUSION

The reactive two-dimensional steady laminar boundary layer flow over a wedge is investigated in this work, with particular attention to the mass and heat transfer of nanofluids using Buongiorno's model. A numerical solution is obtained by combining the RK–Fehlberg method with the shooting method. The impact of physical factors on momentum, energy and concentration profiles is discussed. The effects of various factors on the skin friction coefficient, Nusselt number, and Sherwood number were discussed through tables, and we have the following conclusions:

Velocity profile: The velocity profile increases as the pressure gradient parameter increases, while when the shrinking/stretching wedge parameter increases, velocity decreases.

Temperature profile: The temperature profile increases as the thermophoresis and Brownian motion parameters increase.

Concentration profile: The concentration profiles rise with the rise in the thermophoresis parameter, Brownian motion parameter, and Frank-Kamenetskii number, while the concentration profiles decline with the rise in the activation energy parameter and Lewis number.

Skin friction: As the stretching/contracting wedge parameter and the pressure gradient parameter increase, the skin friction coefficient also rises.

Nusselt number: The Nusselt number upsurges with an upsurge in the factor m, while a decrease in the Nusselt number indicates a decrease in heat transfer efficiency and is brought on by increases in the thermophoretic parameter Nt, Brownian motion parameter Nb, activation energy parameter β, and Lewis number Le.

Sherwood number: Higher values of the Lewis number, thermophoresis parameter, activation energy parameter, and m all result in an increase in the Sherwood number, which denotes a better mass transfer. Nevertheless, as the Brownian motion parameter increases, it decreases.

Future research in this field could go in a number of ways, such as investigating various combinations of nanoparticles in base fluids to improve mass and heat transfer. It could also expand the analysis to three-dimensional flows and non-Newtonian fluids to more closely resemble real-world scenarios. A deeper understanding might be gained by looking into temperature-dependent characteristics, magnetohydrodynamic (MHD) effects, and optimization strategies to maximize heat transfer efficiency. Furthermore, the integration of intricate chemical reactions, phase transition phenomena, and turbulent flow analysis, in conjunction with experimental verification, would enhance the comprehension of the nanofluid behavior and its pragmatic uses in sectors such as manufacturing, environmental engineering, and energy.

ACKNOWLEDGMENTS

The authors extend their appreciation to King Saud University, Saudi Arabia, for funding this work through Researchers Supporting Project No. RSPD2024R704, King Saud University, Riyadh, Saudi Arabia.

AUTHOR DECLARATIONS

Conflict of Interest

The authors have no conflicts to disclose.

Author Contributions

Saeed Ullah Jan: Conceptualization (equal); Methodology (equal); Writing – original draft (equal); Writing – review & editing (equal). **Aatif Ali**: Resources (equal); Visualization (equal); Writing – review & editing (equal). **Mohamed Sharaf**: Data curation (equal); Investigation (equal); Visualization (equal); Writing – review & editing (equal). **Joshua Kiddy K. Asamoah**: Resources (equal); Software (equal); Supervision (equal); Visualization (equal); Writing – review & editing (equal).

DATA AVAILABILITY

The data that support the findings of this study are available within the article.

REFERENCES

[1] V. M. Falkner and S. W. Skan, "Some approximate solutions of the boundary-layer equations," Philos. Mag. **12**, 865–896 (1931).
[2] W. H. H. Banks, "Similarity solutions of the boundary-layer equations for a stretching wall," J. Theor. Appl. Mech. **2**(3), 375–392 (1983).
[3] N. Riley and P. D. Weidman, "Multiple solutions of the Falkner–Skan equation for flow past a stretching boundary," SIAM J. Appl. Math. **49**(5), 1350–1358 (1989).
[4] A. Ishak, R. Nazar, and I. Pop, "Falkner-Skan equation for flow past a moving wedge with suction or injection," J. Appl. Math. Comput. **25**(1–2), 67–83 (2007).
[5] S. U. S. Choi, "Enhancing thermal conductivity of fluids with nanoparticle," in *Developments and Applications of Non-newtonian Flows*, edited by D. A. Siginer and H. P. Wang (ASME, 1995), Vol. 66, pp. 99–105.
[6] J. Buongiorno, "Convective transport in nanofluids," J. Heat Transfer **128**, 240–250 (2006).
[7] Y. Xuan and W. Roetzel, "Conceptions for heat transfer correlation of nanofluids," Int. J. Heat Mass Transfer **43**(19), 3701–3707 (2000).
[8] T. A. Assiri, M. Bilal, E. E. Mahmoud, A. Ali, J. K. K. Asamoah, and A. Adnan, "Numerical investigation of forced convective MHD tangent hyperbolic nanofluid flow with heat source/sink across a permeable wedge," AIP Adv. **14**(6), 065302 (2024).
[9] F. M. Allehiany, M. Bilal, W. F. Alfwzan, A. Ali, and S. M. Eldin, "Numerical solution for the electrically conducting hybrid nanofluid flow between two parallel rotating surfaces subject to thermal radiation," AIP Adv. **13**(7), 075005 (2023).
[10] D. A. Nield and A. V. Kuznetsov, "Boundary layer treatment of forced convection over a wedge with an attached porous substrate," J. Porous Media **9**(7), 683–694 (2006).
[11] R. Saidur, S. N. Kazi, M. S. Hossain, M. M. Rahman, and H. Mohammed, "A review on the performance of nanoparticles suspended with refrigerants and lubricating oils in refrigeration systems," Renewable Sustainable Energy Rev. **15**(1), 310–323 (2011).
[12] O. Mahian, A. Kianifar, S. A. Kalogirou, I. Pop, and S. Wongwises, "A review of the applications of nanofluids in solar energy," Int. J. Heat Mass Transfer **57**(2), 582–594 (2013).
[13] O. Behar, A. Khellaf, and K. Mohammedi, "A review of studies on central receiver solar thermal power plants," Renewable Sustainable Energy Rev. **23**, 12–39 (2013).

[14]D. A. Frank-Kamenetskii, *Diffusion and Heat Transfer in Chemical Kinetics*, 2nd ed. (Plenum Press, New York, 1969).
[15]T. Haroon, A. R. Ansari, A. M. Siddiqui, and S. U. Jan, "Analysis of Poiseuille flow of a reactive power law fluid between parallel plates," Appl. Math. Sci. **5**, 2721–2746 (2011).
[16]A. M. Siddiqui, T. Haroon, S. U. Jan, and B. S. Babcock, "Steady flow of reactive power law fluid in a cylindrical pipe with an isothermal wall," Appl. Math. Sci. **7**, 7037–7051 (2013).
[17]N. A. Yacob, A. Ishak, and I. Pop, "Falkner-Skan problem for a static or moving wedge in nanofluids," Int. J. Therm. Sci. **50**(2), 133–139 (2011).
[18]F. M. White, *Viscous Fluid Flow*, 2nd ed. (McGraw-Hill, New York, 1991).
[19]W. A. Khan and I. Pop, "Boundary layer flow past a wedge moving in a nanofluid," Math. Probl. Eng. **2013**, 637285.
[20]B. L. Kuo, "Heat transfer analysis for the Falkner-Skan wedge flow by the differential transformation method," Int. J. Heat Mass Transfer **48**(23–24), 5036–5046 (2005).
[21]H. Blasius, "Grenzschichten in Flussigkeiten¨ mit kleiner Reibung," Zentralbl. Math. Phys. **56**, 1–37 (1908).
[22]N. Ahmed, U. Khan, S. T. Mohyud-Din, and S. U. Jan, "Non-linear radiative squeezed flow in a rotating frame," Eng. Comput. **34**(8), 2450–2462 (2017).
[23]J. Adler, "Thermal Explosion theory for reactive flow between parallel heated walls," Combust. Flame **24**, 151–158 (1975).
[24]S. S. Okoya, "Thermal stability for a reactive viscous flow in a slab," Mech. Res. Commun. **33**, 728–733 (2006).
[25]U. Khan, N. Ahmed, S. I. U. Khan, and S. T. Mohyud-din, "Thermo-diffusion effects on MHD stagnation point flow towards a stretching sheet in a nanofluid," Propuls. Power Res. **3**(3), 151–158 (2014).
[26]U. Khan, N. Ahmed, M. Asadullah, and S. Tauseef Mohyud-din, "Effects of viscous dissipation and slip velocity on two-dimensional and axisymmetric squeezing flow of Cu-water and Cu-kerosene nanofluids," Propuls. Power Res. **4**, 40 (2015).
[27]T. M. Al-Harthi, A. M. Alqahtani, I. Ragab, R. Alroobaea, A. Rasheed, M. M. M. Abdou, and A. Ali, "Thermal and mass transport investigation of magnetohydrodynamic reactive nanofluid flow utilizing Buongiorno's model," Int. J. Mod. Phys. B **2025**, 2550032.
[28]S. Nasir, A. S. Berrouk, and T. Gul, "Analysis of chemical reactive nanofluid flow on stretching surface using numerical soft computing approach for thermal enhancement," Eng. Appl. Comput. Fluid Mech. **18**(1), 2340609 (2024).
[29]S. Saranya, P. Ragupathi, and Q. M. Al-Mdallal, "Thermal and reactive effects in nanofluid flow around a contracting cylinder under magnetic field influence," Int. J. Thermofluids **22**, 100710 (2024).
[30]A. Dawar, Z. Shah, P. Kumam *et al.*, "Chemically reactive MHD micropolar nanofluid flow with velocity slips and variable heat source/sink," Sci. Rep. **10**, 20926 (2020).
[31]A. Khan, W. Kumam, I. Khan, A. Saeed, T. Gul, P. Kumam, and I. Ali, "Chemically reactive nanofluid flow past a thin moving needle with viscous dissipation, magnetic effects and hall current," PLoS One **16**(4), e0249264 (2021).
[32]Z. Ullah, A. Abbas, E. R. El-Zahar, L. F. Seddek, A. Akgul, and A. M. Hassan, "Significance of thermal density and viscous dissipation on heat and mass transfer of chemically reactive nanofluid flow along stretching sheet under magnetic field," Results Eng. **20**, 101413 (2023).
[33]Z. Khan, W. F. Alfwzan, A. Ali, N. Innab, S. Zuhra, S. Islam, and J. K. K. Asamoah, "Intelligent computing for electromagnetohydrodynamic bioconvection flow of micropolar nanofluid with thermal radiation and stratification: Levenberg–Marquardt backpropagation algorithm," AIP Adv. **14**(3), 035224 (2024).